Diffusion Tensor Echo Planar Imaging Using Surface Coil Transceiver with a Semiadiabatic RF Pulse Sequence at 14.1T

Yohan van de Looij,[1,2] Nicolas Kunz,[1,2] Petra Hüppi,[1] Rolf Gruetter,[2–4]* and Stéphane Sizonenko[1]

Diffusion magnetic resonance studies of the brain are typically performed using volume coils. Although in human brain this leads to a near optimal filling factor, studies of rodent brain must contend with the fact that only a fraction of the head volume can be ascribed to the brain. The use of surface coil as transceiver increases Signal-to-Noise Ratio (SNR), reduces radiofrequency power requirements and opens the possibility of parallel transmit schemes, likely to allow efficient acquisition schemes, of critical importance for reducing the long scan times implicated in diffusion tensor imaging. This study demonstrates the implementation of a semiadiabatic echo planar imaging sequence (echo time = 40 ms, four interleaves) at 14.1T using a quadrature surface coil as transceiver. It resulted in artifact free images with excellent SNR throughout the brain. Diffusion tensor derived parameters obtained within the rat brain were in excellent agreement with reported values. Magn Reson Med 65:732–737, 2011. © 2010 Wiley-Liss, Inc.

Key words: diffusion tensor imaging; ultra-high magnetic field; adiabatic radiofrequency pulse; rat brain; surface coil

Over the last 15 years as a clinical application, diffusion tensor imaging (DTI) has shown remarkable results in a large amount of different pathologies such as the detection of tumors, traumatic brain injury and ischemia, as well as the tracking of brain development (1). Being based on more than only the macroscopic structural contrast of conventional T_1 and T_2 weighted images, DTI gives an additional insight in the brain by probing tissue microstructures. This high interest in DTI for medical diagnostics resulted in a large number of publications.

The brain microstructure information assessed by DTI makes it a complete tool of investigation for preclinical studies on different animal models of disease. Neverthe-less, DTI of the small structures of the rodent brain requires higher resolution in comparison to human studies, decreasing significantly the Signal-to-Noise Ratio (SNR) and thus making DTI on small bore system a very challenging technique. It results in a very small number of publications focused on the rat brain (2–10) compared to the numerous human studies (1) found in the literature. To compensate for the loss of SNR of this very time consuming technique, the established solution was the use of ultra high magnetic field for its intrinsic gain in SNR combined with fast imaging technique such as echo planar imaging (EPI). EPI is routinely used to accelerate the acquisition time and to reduce motion artifacts. The improvement in SNR achievable with increasing static magnetic field, makes ultrahigh magnetic field systems (>7T) attractive for DTI applications, despite the enhancement of the major drawbacks of EPI related to susceptibility artifacts through slice signal dephasing and geometric distortions. Such artifacts can be reduced by decreasing the echo time (TE) and EPI read-out time, respectively. This can be achieved either by using segmented read-out EPI or parallel imaging. Another common EPI artifact, Nyquist ghosting, can be minimized by adding images acquired with a positive and a negative read-out gradient and their respective reference phase scans (11).

All of the recent rat studies (2–10) have been performed at 7T or below with a volume coil as transmitter and receiver for homogeneous excitation, or volume coil as transmitter and surface coil as receiver for homogeneous excitation and better sensitivity during reception. However, the higher power requirement of a volume coil at 14.1T could be an issue with regard to the necessity of a more powerful radiofrequency (RF) amplifier when compared to a surface coil. Surface coils as transmitter and receiver are generally not used in MRI due to their inhomogeneous excitation, resulting in a loss of signal distal from the RF coil. Surface coil transmit B_1 inhomogeneities can be attenuated by using adiabatic RF pulses, providing a better coverage of the imaged sample without any modification of the hardware system or animal set-up. A fully adiabatic double spin-echo sequence for DTI used with surface coil has been previously proposed in a single slice or a 3D volume acquisition scheme (12).

The use of a single coil positioned on top of the brain, provides an easier access to the subject, facilitating grandly the preparation and the monitoring of the animal compared to volume coil set-up. In addition, their high performance in regions close to the coil fulfills the
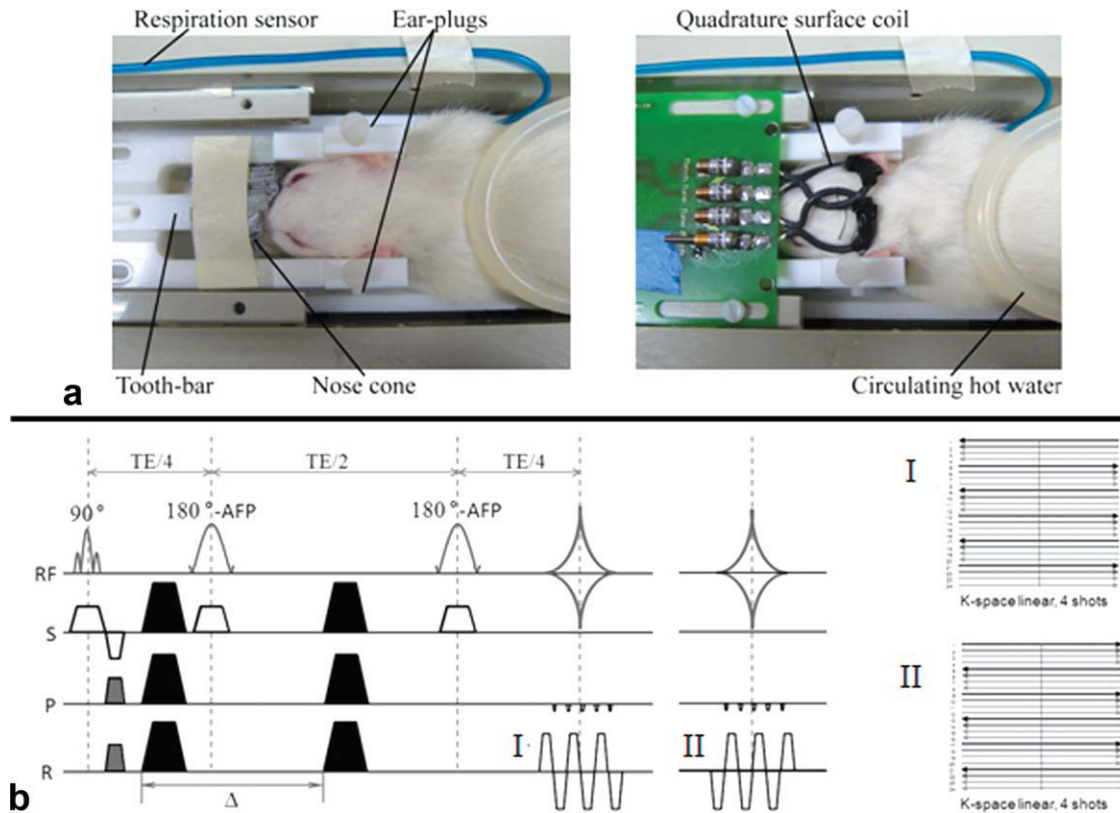
FIG. 1. Experimental setup showing the stereotaxic fixation (ear-plugs and tooth-bar), the respiration sensor, the circulating hot water, the nose cone for isoflurane anesthesia and the quadrature surface coil. **B**: Semiadiabatic double spin-echo sequence. White (slice selection) and gray (prephasors for the EPI readout) gradients are part of the imaging scheme, while black gradients are used for the diffusion encoding. On the right positive (I) and negative (II) read-out gradients and the corresponding *k*-space trajectories to cancel Nyquist ghosting artifacts are shown. [Color figure can be viewed in the online issue, which is available at wileyonlinelibrary.com.]

requirement of localized proton magnetic resonance spectroscopy (MRS) and has proved its relevance in investigation of various cerebral pathologies.

Therefore, the aim of this work was to develop a diffusion tensor EPI sequence with conventional hardware equipment at 14.1T for in vivo studies.

MATERIALS AND METHODS

During measurements, each adult Wistar rat ($n = 4$) was anesthetized with 1.5–2% isoflurane in O_2 and subsequently placed supine within an adapted holder, while the head was stereotaxically fixed via ear bars (Fig. 1A). Body temperature was maintained at 37°C using thermo-regulated water circulation.

All in vivo MR experiments were performed on a 14.1T/26 cm magnet (Magnex Scientific, Oxford, UK) connected to Direct Drive console (Varian Medical Systems, Palo Alto, CA) equipped with 12-cm gradient coils (400 mT/m in 120 μs), a RF amplifier of 100 W (model 3900C, Herley Industries, Lancaster, PA) and a quadrature transmit-receive surface RF coil composed of two loops of 18 mm diameter (Fig. 1A).

Fast spin-echo (FSE) images were acquired for reference (FOV = 23 × 23 mm^2, Matrix = 256 × 128, TE/TR = 60/6000 ms, eight averages, slice thickness = 0.8 mm, echo train length = 16). First and second order shims were adjusted using FASTMAP (13), resulting in a water linewidths of 18 to 22 Hz for a voxel of 5 × 7 × 7 mm^3 centered in the brain.

A semiadiabatic (conventional 90° RF pulse for excitation and adiabatic full passage pulse for refocusing) double spin-echo segmented EPI sequence (Fig. 1B) was implemented. The refocusing RF pulses were slice-selective adiabatic full passage of the hyperbolic secant type (HS180: bandwith = 6.4 KHz, duration = 2.5 ms, cutoff = 1%) (14). The second HS180 was applied to cancel the quadratic through-slice phase dependence (13). Eight slices of 0.8 mm thickness with a field of view of 23 × 15 mm^2 were sampled on a 128 × 64 (RO × PE) Cartesian grid using a 4 shot interleaved EPI k-space acquisition (TE/TR = 40/4000 ms, 10 averages). No phase correction was applied to account for shot-to-shot phase errors. Nyquist ghosting artifacts were minimized by adding images acquired with a positive and a negative read-out gradient train (i.e., repetition with the entire read-out EPI train inverted) after each had been corrected by their respective reference phase scans (Fig. 1B) (11).

To compare performances of the semiadiabatic sequence, additional images were acquired with a single spin-echo four shot EPI sequence (i.e., with sinc-shaped pulses) with the same parameters except TE optimized with respect to the diffusion parameters used in this study (see below) and reduced to 30 ms.
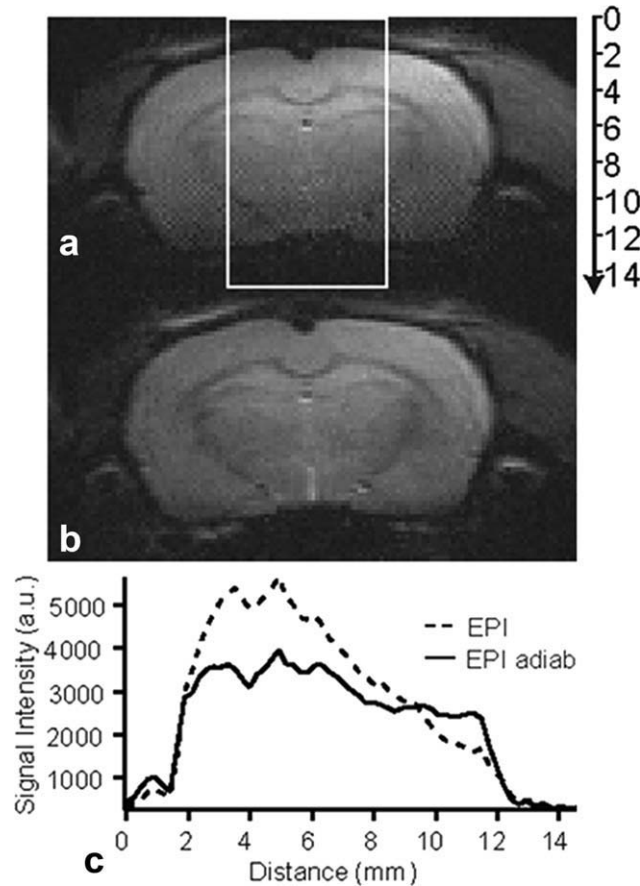
FIG. 2. Standard single spin-echo EPI image (**A**) with minimal TE allowing diffusion experiments with $\delta/\Delta = 3/20$ ms (four shot, field of view = 23×15 mm^2, Matrix = 128×64, TE/TR = 30/2000 ms, nb of averages = 2, slice thickness = 1 mm), semiadiabatic double spin-echo image (**B**) with the same parameters except the TE set to 40 ms and (**C**) vertical profile in the ROI drawn on image A.

To minimize the TE in the semiadiabatic sequence, diffusion gradients were applied with the same polarity about the first HS180 pulse (Fig. 1B) with the following parameters: intensity (G), duration (δ) and diffusion time (Δ) were set to 290 mT/m, 3 ms, and 20 ms, respectively; resulting in a b-value of 1030 s mm^{-2}. Forty-two spatial directions were sampled to improve the accuracy of the anisotropy measurements (15). The sampling scheme consisted of 21 Icosahedral directions as well as their 21 opposites to cancel cross terms caused by sequence-specific coherence-selective gradients (16). The cancellation of the b-value cross terms was obtained by taking the square root of the product of signal from opposite directions. The acquisition time per gradient direction was less than 3 minutes for a total acquisition time <2 hours.

Diffusion-weighted images were reconstructed and zero-filled to a 256×168 matrix using Matlab (Mathworks, Natick, MA). Diffusivity values apparent diffusion coefficient (ADC, $D_{//}$ and $D_{\perp}$) as well as the fractional anisotropy (FA) were derived from diagonalization of the diffusion tensor.

Six different ROIs were manually delineated and analyzed: the corpus callosum (CC), the cortex (Cx), the external capsule (EC), the cranial nerves (CN), the ven-

tricles (Ven) and cerebrospinal fluid at the bottom of the brain (CSF) (Fig. 3). To minimize potential partial volume effects, the ROIs were carefully delimited on color maps and restricted to the inner part of the different brain structures analyzed. To visualize the orientation of the fiber bundles, direction encoded color maps were generated based on the principal eigenvector direction.

All image SNRs were calculated from the ratio of $<S_{tissue}>$, the mean signal intensity in a region of the brain (i.e., Cx and striatum) obtained from the reference image (b_0), relative to SD$_{noise}$, the standard deviation of a large ROI positioned in the background noise that was visually devoid of artifacts.

RESULTS

Anatomical images acquired with the semiadiabatic double spin sequence (Fig. 3) showed whole brain coverage and excellent contrast. In fact, quality and anatomical information in the EPI images were remarkably consistent with and comparable to the FSE images (Fig. 3): (i) the T_2 weighted contrast of the EPI sequence was equally suitable for delineation of white and gray matter; (ii) the nominal in-plane resolution (180×230 μm^2) was sufficient to clearly define anatomic brain structures. In addition, no significant geometrical distortions or susceptibility artifacts were noticed in the EPI images, even in critical regions such as the interface between brain and skull and close to air, such as the sinuses. Nyquist ghosting was minimized to the noise level by the use of opposite gradient read-out scheme (11), improving the overall image quality significantly (Fig. 2A). Adding strong diffusion gradients ($\delta/\Delta = 3/20$ ms with $b = 1030$ s/mm^2), resulted in diffusion-weighted images, that remained free of artifacts or geometric distortions (data not shown).

EPI artifacts such as geometric distortion, T_2 losses and blurring in the phase encoding direction due to T_2^*, which are particularly important at 14.1T, were minimized by optimizing spectral width, TE and the number of segments. To reduce the TE, diffusion gradients were applied around the first HS180 refocusing pulse (Fig. 1B) allowing for time for the EPI read-out. Consequently, the EPI read-out, being the only module present in the last TE/4 period of the sequence, was the main determining factor for the minimal TE possible. The experiment was designed as a four-shot read-out EPI acquisition to reduce the read-out time by fourfold, resulting in an TE of 40 ms (with $\Delta \leq 20$ ms). In accordance with the previous efforts to reduce the TE, and especially geometric distortions, spectral width was set to 250 kHz with an echo-spacing equal to 0.65 ms. In addition, B_0 inhomogeneities were compensated by automatically adjusting the first and second order of shims (13), which has been proven to clearly reduce susceptibility artifacts and geometric distortions (17).

When comparing the single spin-echo EPI sequence (TE = 30ms) to the semiadiabatic EPI version (TE = 40ms) (Fig. 2A and B, respectively), an obvious improvement in coverage of the deeper regions of the brain was noticed. According to the shorter TE and thus reduced T_2 losses, the profile of the conventional EPI image (dashed line Fig. 2C) showed a net gain in signal in the

Table 1
Mean Values ± SD of ADC, $D_{//}$, $D_{\perp}$, and FA in Different ROIs: Corpus callosum (CC), Cortex (Cx), External capsule (EC), Cranial Nerves (CN), Ventricles (Ven) and CSF in the Deeper Part of the Brain (CSF)

	CC	Cx	EC	CN	Ven	CSF
ADC	6.8 ± 0.6	7.4 ± 0.2	7.1 ± 0.2	9.0 ± 0.8	23.1 ± 1.3	22.8 ± 3.6
$D_{//}$	15.7 ± 1.4	9.4 ± 0.3	11.2 ± 0.4	14.3 ± 1.8	25.4 ± 1.8	24.0 ± 3.2
$D_{\perp}$	2.3 ± 0.2	6.4 ± 0.2	5.0 ± 0.3	6.3 ± 0.5	21.9 ± 1.0	21.8 ± 3.6
FA	0.84 ± 0.02	0.25 ± 0.01	0.48 ± 0.04	0.47 ± 0.05	0.10 ± 0.02	0.08 ± 0.02

Except of FA, all values are expressed $\times 10^{-4}$ mm^2/s.

upper parts of the brain followed by a strong attenuation due to the sine cube dependence of the excitation profile B_1 (18). On the other hand, the projection along the axis of the RF coil of the semiadiabatic EPI sequence (solid line Fig. 2C) was nearly flat, in accordance to the sine B_1 dependence of the excitation pulse (18).

SNR values measured in the Cx on the b_0 and DW-images were 50 ± 6 and 36 ± 7, respectively; a reduction by a factor of 1.4. The same signal decrease was observed in the striatum with SNR values of 24 ± 7 and 18 ± 5 in b_0 and DW images, respectively. Mean values of ADC, $D_{//}$, $D_{\perp}$ and FA (Table 1) were averaged in several rat brain structures indicated in Figure 3. The FA maps showed excellent contrast between white and gray matter according to anisotropic differences, even in the deeper

parts of the brain such as CN. In addition, direction encoded color maps showed clearly the preferred direction of diffusion. Indeed, the radial organization of the Cx was observed (green, then red from the hemisphere junction to the rhinal fissure) with a low FA value of 0.25 ± 0.01 (ADC = 7.4 ± 0.2 × 10^{-4} mm^2/s).

The CC, with a measured FA value of 0.84 ± 0.02 (ADC = 6.8 ± 0.6 × 10^{-4} mm^2/s), appeared dark red on the maps, reflecting the well known right-left fiber organization. The CN (blue), situated at the deeper part of the brain, presented a FA value of 0.47 ± 0.05 (ADC = 9.0 ± 0.8 × 10^{-4} mm^2/s) with a front-rear orientation (blue). In the ventricle as well as CSF at the deeper part of rat brain, diffusion tensor derived parameters presented values close to the ones of free water (ADC =
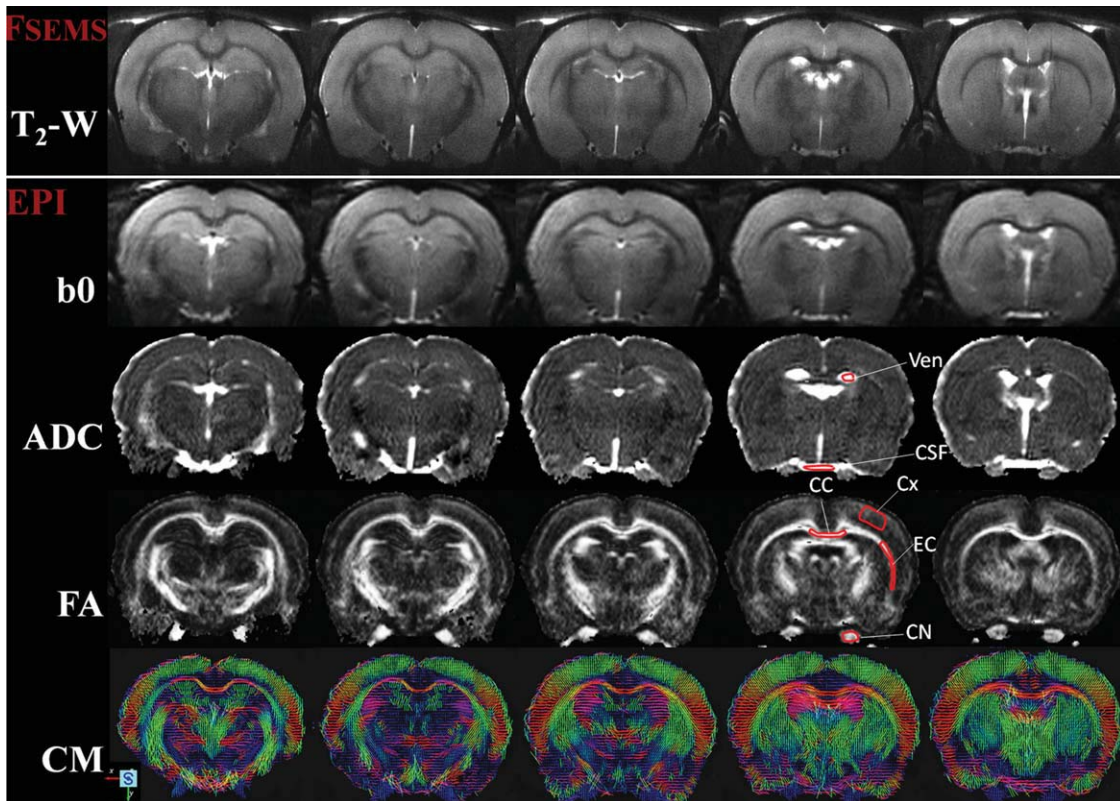

FIG. 3. FSE images (T_2-W: field of view = 23 × 23 mm^2, Matrix = 256 × 128, TE/TR = 60/6000 ms, nb of averages = 8, slice thickness = 0.8 mm, echo train length = 16) and DTEPI indices maps obtained with the semiadiabatic sequence. Typical EPI b_0 images (b_0), apparent diffusion coefficient maps (ADC), fractional anisotropy maps (FA) and color maps (CM) of an adult rat brain. On the fourth FA map from the left, the ROIs for the measurement of DTI derived parameters in the corpus callosum (CC), cortex (Cx), ventricle (Ven), Cerebro Spinal Fluid at the deeper part of the brain (CSF), external capsule (EC) and cranial nerve (CN) are displayed. Images show a complete coverage of the adult rat brain with a high SNR.

23.1 ± 1.2 × 10^{-4} mm²/s; FA = 0.1 ± 0.02 and ADC = 22.8 ± 3.6 × 10^{-4} mm²/s; FA = 0.08 ± 0.02, respectively).

DISCUSSION

This study demonstrates that diffusion-weighted images acquired with the proposed semiadiabatic double spin-echo sequence provide good coverage of the brain even when using surface coil as transceiver. Furthermore, a reliable reconstruction of the diffusion tensor was possible at 14.1T, where EPI images were notably free of major artifacts and showed excellent contrast between white and gray matter brain structures.

The HS180 pulses, when used in the adiabatic regime, provide a better inversion in the parts of the brain that are located further from the coil (14) improving the coverage of the brain compared with conventional spin-echo EPI sequence (sinc-shaped pulses) (Figs. 2A and B). In addition, deep brain structures such as, amygdala, hypothalamus or the third ventricle, were clearly identifiable in the semiadiabatic EPI image.

The pulse sequence presented in this study resulted in images providing a complete coverage of the brain in the rostro-caudal direction and an SNR ≥24 throughout the entire brain on the b_0 images, which, should lead to an accurate estimation of the diffusion-tensor derived parameters (19). In addition, for regions with intrinsic low FA, it has been shown that noisy DTI data sets contain a positive bias in the FA values (20), therefore, we believe that the low FA in the ventricles demonstrated the excellent quality of the data. Also, the same range of FA values was found in CSF at the deeper part of the brain as in the ventricles, proving the good coverage of the entire brain with excellent quality of tensor reconstruction even at the base of the image.

It is important to notice that the proposed EPI based sequence shows images free of artifacts, which is even more remarkable at such high magnetic field of 14.1T. The optimization of the read-out parameters (spectral bandwidth and multishot acquisition), in combination with the double spin-echo preparation, resulted in images equivalent to FSE in terms of quality and contrast, where no significant geometric distortions and susceptibility artifacts were visible (Fig. 3). In addition, Nyquist ghosting artifacts were significantly reduced by using an alternated read-out gradient polarity acquisition (11).

B_1 inhomogeneities, engendered by the use of surface coil as transmitter and receiver, resulted in loss of signal along the cranial-caudal direction. Therefore, the cone of sensitivity of the surface coil was limited to the brain, with minimal contribution of tissues underneath as judged from the absence of aliasing in the top of the b_0 image in Figure 3. Consequently, it was possible to reduce the field of view in the phase encoding direction, along the cranial-caudal direction, allowing an isotropic in plane resolution with a reduced number of phase encoding steps. The bias in the signal intensity had no impact on diffusion tensor computation, as the images were rescaled with respect to the b_0 reference image. Diffusion-weighted images (data not shown), acquired with

Table 2
Overview of the Recent Rat DTI Studies at High Magnetic Field (≥3T) Found in the Literature

References	Application	Field	Coil	Seq.	Resolution	TR/TE	Diff. Sc	Time	FA CC	ADC CC	FA Cx	ADC Cx
This study	Methodology	14.1T	Surf	EPI, 4s	0.18 × 0.23 × 0.8	4000/40	2 × 21	<2h	0.84 ± 0.02	6.8 ± 0.6	0.25 ± 0.01	7.4 ± 0.2
2	Tumor	7T	Vol, Surf	EPI, 4s	0.2 × 0.2 × 1	3000/50	30	70 min	–	–	~ 0.2	~ 5.5
8	Ischemia	4.7T	Vol, Surf	EPI, 8s	0.25 × 0.25 × 1	3000/32	6	–	No absolute values			
5	Tumor	4.7T	Vol, Surf	SE	0.16 × 0.16 ×-	2000/56	6	3 h	~ 0.75 ± 0.02	–	–	–
4	Stroke	7T	Vol, Surf	SE	0.25 × 0.25 × 1	1500/40	6	45 min	No absolute values			
10	Tumor	4.7T	Vol, Surf	SE	0.33 × 0.33 × 1	2000/57	6	2 h	Values measured in striatum and tumors			
6	Tracking	3T	**	EPI	0.5 × 0.5 × 0.5	2000/33	2 × 6	92 min	0.35–0.45	5.9–8.3	–	–
9	Tracking	–	–	FSE	0.11 × 0.16 × 0.26	1000/–	6	2h	No absolute values			
7*	Ischemia	4.7T	Vol	SE	0.13 × 0.13 × 0.5	1500/40	6	4 h	Values measured at 6 days-old			
3*	Development	7T	Vol, Surf	EPI, 4s	0.27 × 0.27 × 0.5	4000/38	2 × 21	50 min	0.68 ± 0.10	8.1 ± 0.7	0.13–0.29	7.4–7.7

First row is about this study. Resolutions and TE/TR are expressed in mm³ and ms, respectively. Abbreviations: Seq: Sequence, 4s: 4 shots, Diff. Sc.: diffusion scheme (i.e. number of directions).

*: pups study; **: insert gradient coil. ADC values are expressed ×10^{-4} mm²/s.

strong intensity gradients (G = 290 mT/m) and a short duration (δ = 3 ms), showed the same quality as the anatomical images described previously, suggesting that eddy current effects were negligible.

FA maps and direction encoded color maps were in excellent agreement with previous studies (3). A large variability in published diffusion indices was noted, making a direct comparison with this study challenging (Table 2). For example, FA values in the rodent CC varied from 0.4 to 0.8 (Table 2). However, ADC and FA values (Table 1) were highly consistent for all other brain structures, such as Cx. The variation in published values can be explained by the dependence on ROI position (partial volume effects) and differences in acquisition protocols (i.e., diffusion time, gradient application time, gradient scheme, etc) and magnetic field strength (19).

It should be noticed that parallel imaging may help reduce most of the problem enounced earlier such as scan time, excitation coverage and sensitivity. Nevertheless, it involves specific hardware such as multiple receiver channels and arrayed surface coils, which still remains technically difficult to build and is rarely directly available on small bore magnets. However, the proposed sequence leads itself to be implemented with a multiple coil transceiver array for parallel imaging and parallel transmission, which should provide additional gain in acquisition time.

CONCLUSION

We conclude that using a surface coil as transmitter and receiver, it is feasible for DT-EPI of the rat brain in vivo at 14.1T with whole brain coverage. The data shows rich structural details, not only of white matter but also of gray matter, which could allow achievement of segmentation and volumetric measurements. The implementation of the proposed EPI based sequence at lower magnetic field is possible and may provide interesting features despite a loss of SNR. The possibility to combine the in vivo DTI protocol, presented in this study, with localized ^{1}H-MRS provides a powerful multimodal tool that merges brain microstructure information and localized neurochemical information.

REFERENCES

1. Sundgren PC, Dong Q, Gomez-Hassan D, Mukherji SK, Maly P, Welsh R. Diffusion tensor imaging of the brain: review of clinical applications. Neuroradiology 2004;46:339–350.

2. Asanuma T, Doblas S, Tesiram YA, Saunders D, Cranford R, Pearson J, Abbott A, Smith N, Towner RA. Diffusion tensor imaging and fiber tractography of C6 rat glioma. J Magn Reson Imaging 2008;28:566–573.

3. Bockhorst KH, Narayana PA, Liu R, Ahobila-Vijjula P, Ramu J, Kamel M, Wosik J, Bockhorst T, Hahn K, Hasan KM, Perez-Polo JR. Early postnatal development of rat brain: in vivo diffusion tensor imaging. J Neurosci Res 2008;86:1520–1528.

4. Ding G, Jiang Q, Li L, Zhang L, Zhang ZG, Ledbetter KA, Panda S, Davarani SP, Athiraman H, Li Q, Ewing JR, Chopp M. Magnetic resonance imaging investigation of axonal remodeling and angiogenesis after embolic stroke in sildenafil-treated rats. J Cereb Blood Flow Metab 2008;28:1440–1448.

5. Lope-Piedrafita S, Garcia-Martin ML, Galons JP, Gillies RJ, Trouard TP. Longitudinal diffusion tensor imaging in a rat brain glioma model. NMR Biomed 2008;21:799–808.

6. Mayer D, Zahr NM, Adalsteinsson E, Rutt B, Sullivan EV, Pfefferbaum A. In vivo fiber tracking in the rat brain on a clinical 3T MRI system using a high strength insert gradient coil. NeuroImage 2007;35:1077–1085.

7. Sizonenko SV, Camm EJ, Garbow JR, Maier SE, Inder TE, Williams CE, Neil JJ, Huppi PS. Developmental changes and injury induced disruption of the radial organization of the cortex in the immature rat brain revealed by in vivo diffusion tensor MRI. Cereb Cortex 2007;17:2609–2617.

8. van der Zijden JP, van der Toorn A, van der Marel K, Dijkhuizen RM. Longitudinal in vivo MRI of alterations in perilesional tissue after transient ischemic stroke in rats. Exp Neurol 2008;212:207–212.

9. Xue R, van Zijl PC, Crain BJ, Solaiyappan M, Mori S. In vivo three-dimensional reconstruction of rat brain axonal projections by diffusion tensor imaging. Magn Reson Med 1999;42:1123–1127.

10. Zhang J, van Zijl PC, Laterra J, Salhotra A, Lal B, Mori S, Zhou J. Unique patterns of diffusion directionality in rat brain tumors revealed by high-resolution diffusion tensor MRI. Magn Reson Med 2007;58:454–462.

11. van der Zwaag W, Marques JP, Lei H, Just N, Kober T, Gruetter R. Minimization of Nyquist ghosting for echo-planar imaging at ultra-high fields based on a "negative readout gradient" strategy. J Magn Reson Imaging 2009;30:1171–1178.

12. Ronen I, Kim KH, Garwood M, Ugurbil K, Kim DS. Conventional DTI vs. slow and fast diffusion tensors in cat visual cortex. Magn Reson Med 2003;49:785–790.

13. Gruetter R, Tkac I. Field mapping without reference scan using asymmetric echo-planar techniques. Magn Reson Med 2000;43:319–323.

14. Conolly S, Glover G, Nishimura D, Macovski A. A reduced power selective adiabatic spin-echo pulse sequence. Magn Reson Med 1991;18:28–38.

15. Jones DK. Determining and visualizing uncertainty in estimates of fiber orientation from diffusion tensor MRI. Magn Reson Med 2003;49:7–12.

16. Madi S, Hasan KM, Narayana PA. Diffusion tensor imaging of in vivo and excised rat spinal cord at 7 T with an icosahedral encoding scheme. Magn Reson Med 2005;53:118–125.

17. Lei H, Mlynarik V, Just N, Gruetter R. Snapshot gradient-recalled echo-planar images of rat brains at long echo time at 9.4 T. Magn Reson Imaging 2008;26:954–960.

18. Bernstein M, King K, Zhou X. Handbook of MRI pulse sequences. Boston: Elsevier Academic Press; 2004. 1040 p.

19. Qin W, Yu CS, Zhang F, Du XY, Jiang H, Yan YX, Li KC. Effects of echo time on diffusion quantification of brain white matter at 1.5 T and 3.0 T. Magn Reson Med 2009;61:755–760.

20. Jones DK, Basser PJ. Squashing peanuts and smashing pumpkins: how noise distorts diffusion-weighted MR data. Magn Reson Med 2004;52:979–993.